Pergamon

Cement and Concrete Research 29 (1999) 679–686

CEMENT AND CONCRETE RESEARCH

Transmission electron microscopic study of ferrite in sulfate-resisting Portland cement clinker[1]

Angel R. Landa-Cánovas [a], Staffan Hansen [b,*]

[a]*Centro de Microscopia Electronica "Luis Bru," Universidad Complutense de Madrid, E-28040 Madrid, Spain*
[b]*National Center for HREM, Inorganic Chemistry 2, Chemical Center, Lund University, P.O. Box 124, S-221 00 Lund, Sweden*

Manuscript received 20 November 1998; accepted manuscript 21 January 1999

Abstract

The oxide interstitial material in industrial clinker for sulfate-resisting Portland cement was extracted using salicylic acid and investigated by transmission electron microscopy and X-ray powder diffraction (XRD). The orthorhombic unit cell parameters of the ferrite phase were determined for two samples by XRD: (1) a = 5.529, b = 14.542, c = 5.347 Å; and (2) a = 5.550, b = 14.526, c = 5.347 Å. Energy dispersive X-ray microanalysis indicated that the ferrite normally had an atomic Al/Fe ratio of 0.7–0.9 and an average composition of $Ca_{2.03}Al_{0.72}Fe_{0.87}Mg_{0.11}Mn_{0.05}Si_{0.17}Ti_{0.03}O_5$ (13 analyses). Sometimes the composition varied on the micrometer scale, and areas with Al/Fe approaching 2 were observed. Electron diffraction indicated the basic structure to be of symmetry Ibm2, each layer of Bragg spots perpendicular to c* being accompanied by a sheet of diffuse intensity. It is proposed that the diffuse scattering is generated by a disordered array of single tetrahedral chains with reversed polarity in the brownmillerite-type crystal structure.

Keywords: Crystal structure; Transmission electron microscopy; Calcium aluminoferrite; Clinker; Sulfate-resistant cements

The rheology of freshly prepared concrete is influenced by the rapidly forming hydration products of aluminate (substituted $Ca_3Al_2O_6$) and ferrite (substituted Ca_2AlFeO_5) in Portland cement. For heavy constructions in contact with sea water, sulfate-resisting Portland cement (SRPC) is widely used. In SRPC, ferrite is the dominant interstitial phase compared to aluminate. In ordinary Portland cement (OPC), aluminate and ferrite occur in similar amounts. The hydration reactions of pure synthetic aluminates and ferrites have been reviewed [1]. The reaction products of clinker aluminate and ferrite in OPC and SRPC also have been investigated [2,3]. Recently, we studied the hydration kinetics of Ca_2AlFeO_5 in the presence of bases and sulfates [4], the distribution of iron among the resulting product phases [5], and the early hydration of model cements containing ferrites $Ca_2(Al_xFe_{1-x})_2O_5$ (x = 0.0, 0.28, 0.34, 0.50, 0.67) and production SRPC [6]. A previous study [7] of Swedish SRPC clinker by elemental mapping and scanning electron microscopy showed that the aluminate could only rarely be distinguished from the ferrite in the interstitial material, due to the low amount present and the small size of the crystals. Because crystal defects can increase the reactivity of a solid and diffuse scattering in the electron diffraction patterns of ferrite from oil-well cement clinker has been reported [8], the present transmission electron microscopic investigation of SRPC ferrite was undertaken.

1. Experimental

1.1. Preparation of samples

Swedish industrial clinkers for SRPC and OPC were ground to an average grain size of 5 μm. To selectively extract the interstitial oxides, the powder was stirred with salicylic acid dissolved in methanol for 24 h, vacuum filtered, and washed with acetone.

1.2. X-ray powder diffraction

Extracted interstitial material was mixed with Si and mounted on Scotch tape. X-ray powder diffraction films were obtained using a Guinier-Hägg camera (CuKα1 radiation). Approximate lattice parameters for the ferrite phase were determined using reflections with convenient indices and the parameters were refined using the least-squares method and Si reflections for internal calibration.

* Corresponding author. Tel.: 46-46-222-8117; Fax: 46-46-222-4012; E-mail: staffan.hansen@oorg2.lth.se.

[1] This paper was originally submitted to *Advanced Cement Based Materials* in February 1998. The paper was received at the Editorial Office of *Cement and Concrete Research* on 20 November 1998 and accepted in final form 21 January 1999.

0008-8846/99/$–see front matter
PII: S0008-8846(99)00031-9

Table 1
Orthorhombic unit cells of different clinker ferrites and synthetic Ca_2AlFeO_5*

Sample	a/Å	b/Å	c/Å
SRPC 1	5.529 (3)	14.542 (6)	5.347 (4)
SRPC 2	5.550 (1)	14.526 (4)	5.347 (2)
OPC 1	5.536 (9)	14.541 (16)	5.362 (8)
OPC 2	5.541 (2)	14.516 (5)	5.328 (2)
Ca_2AlFeO_5	5.560 (1)	14.511 (2)	5.343 (1)

* Estimated standard deviations referring to the last digit(s) are given in parentheses.

1.3. Electron microscopy

The extracted phases from SRPC clinker were dispersed on copper grids covered with holey carbon film and examined by imaging and diffraction techniques using a JEM-2000FX transmission electron microscope, operated at 200 kV and equipped with a Link AN10000 energy dispersive X-ray microanalysis (EDX) system. Elemental analysis was carried out with an effective counting time of 100 s and a typical spot size of 0.1 μm.

2. Results and discussion

2.1. Substitutions

The lattice parameters (Table 1) of the ferrites from Swedish SRPC and OPC are similar to each other and to those determined for synthetic Ca_2AlFeO_5 using powder X-ray diffraction methods. However, elemental analysis by EDX indicates that about one fifth of the trivalent ions in the SRPC clinker ferrites are substituted by other ions as compared to ideal Ca_2AlFeO_5. The replacement appears to be of the type $2\,M(3+) \leftrightarrow M(2+) + M(4+)$, where $M(3+)$ = Al, Fe; $M(2+)$ = Mg, Mn; and $M(4+)$ = Si, Ti. The analyses usually exhibit an atomic ratio Al/Fe in the range of 0.7–0.9. From 13 analyses in this range, an average composition of $Ca_{2.03(9)}Al_{0.72(6)}Fe_{0.87(5)}Mg_{0.11(2)}Mn_{0.05(1)}Si_{0.17(6)}Ti_{0.03(1)}O_5$ was calculated (estimated standard deviations in parentheses).

This result is similar to the average composition obtained by EDX analysis on the same sample using the scanning electron microscope [7], i.e., $Ca_{2.01}Al_{0.71}Fe_{0.89}Mg_{0.08}Mn_{0.05}Si_{0.16}Ti_{0.03}O_5$. Similar levels of the major substituting ions have been reported in other EDX studies of ferrite in SRPC [3] and oil-well cement [8,9] clinker. The oxidation state of manganese has been reported as being divalent [8] or trivalent [3], although the content is low. The results of the present study suggest that manganese should be divalent to obtain the best charge balance. Nevertheless, the Mn(III) compound Ca_2AlMnO_5 has been prepared [10].

Due to the superior spatial resolution of analyses performed in the transmission electron microscope, areas richer in Al occasionally could be observed (Fig. 1). Thus, substantial variation in the Al/Fe ratio can occur on the micrometer scale. The analysis with maximum aluminium

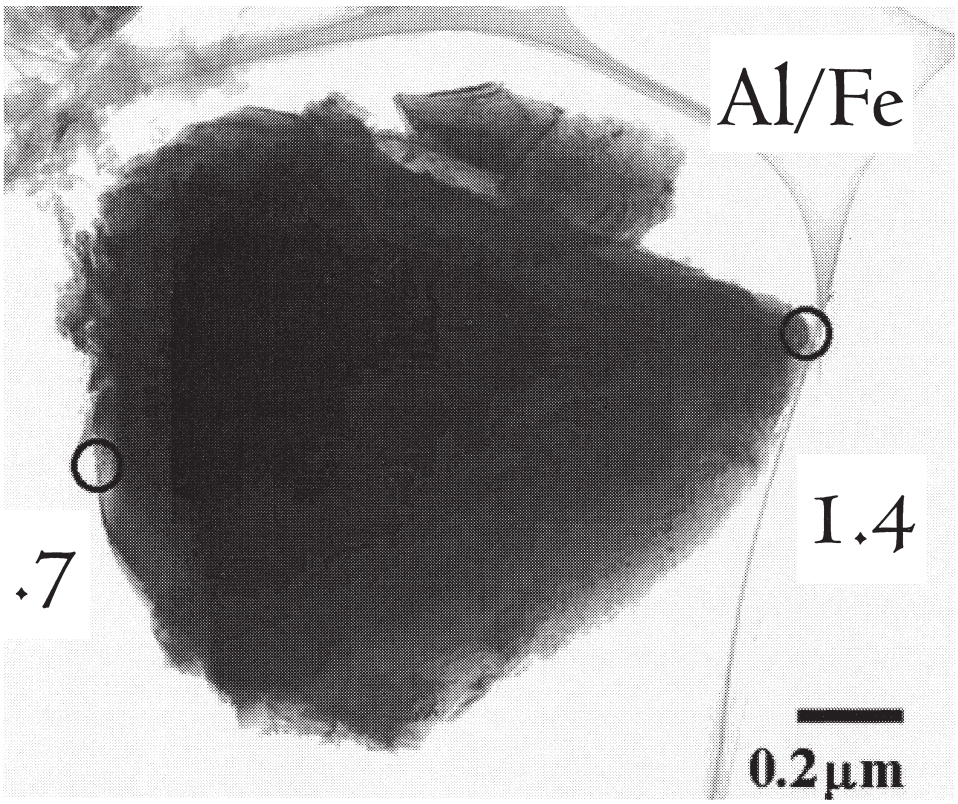

Fig. 1. Ferrite grain exhibiting large variation in composition. EDX analysis of the circled areas gave Al/Fe atomic ratios of 0.7 (left) and 1.4 (right). Values approaching 2 have been observed, but values around 0.8 are the most common.

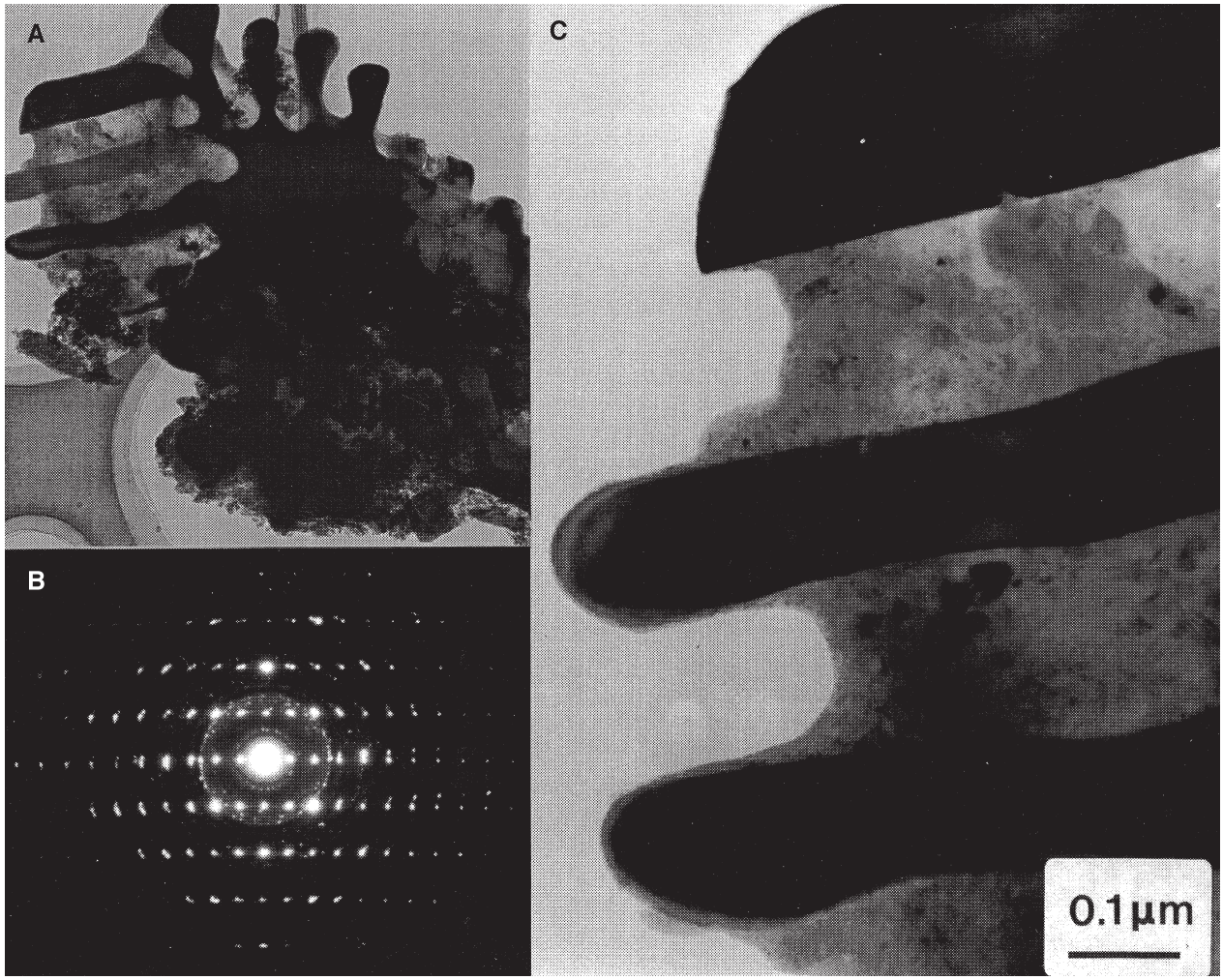

Fig. 2. (*A*) Dendritic ferrite crystal. (*B*) Electron diffraction pattern of dendrite branches showing a spot pattern from ferrite, zone axis [1 0 −1], and superimposed powder diffraction rings from aluminate. (*C*) Magnification revealing intergrowth of ferrite (dark) and polycrystalline aluminate (light).

content observed (Al/Fe = 1.90) resulted in the composition $Ca_{1.96}Al_{1.20}Fe_{0.63}Mg_{0.06}Mn_{0.03}Si_{0.09}Ti_{0.01}O_5$, which suggests that Al-rich areas are less substituted by divalent and tetravalent ions. Similar short-range variations in composition of the ferrite phase have been reported for oil-well cement clinker [8]. The segregation of Al-rich ferrite at the surface of crystals also has been observed by visible light microscopy [11] and surface analysis [12].

How the presence of different dopant ions in the ferrite crystals will affect their hydration properties is hard to predict a priori and has to be determined empirically. Hydration experiments on synthetic members of the series $Ca_2(Al_xFe_{1-x})_2O_5$; $0 < x < 0.67$, has shown that the reaction rate increases with increasing content of aluminium, in pure water and saturated $Ca(OH)_2$ solution [13], as well as in the presence of gypsum and alite [6]. The substitution of Fe(3+) by 1/2 Mg(2+) + 1/2 Si(4+) in Ca_2AlFeO_5 was shown [14] to be difficult to achieve in synthetic samples prepared using MgO and low quartz at 1150–1300°C.

2.2. Dendritic ferrite

In the transmission electron microscope, the ferrite usually appeared in well-defined grains as depicted in Fig. 1, whereas the aluminate was much rarer. Nevertheless, ferrite in the well-known dendritic shape also was observed (Fig. 2A). By increasing the magnification, a fine-grained material filling the interstices of the dendrite could be observed (Fig. 2C). Qualitative EDX and selected area electron diffraction (Fig. 2B) identified this polycrystalline material as aluminate, i.e., substituted $Ca_3Al_2O_6$.

2.3. Basic crystal structure

At ambient pressure, the synthetic series $Ca_2(Al_xFe_{1-x})_2O_5$ can be prepared [15,16] with compositions extending from $x = 0$ to $x = 0.7$. The crystal structure of the pure iron end member $Ca_2Fe_2O_5$ is primitive orthorhombic [17], whereas that of Ca_2AlFeO_5 is body-centered orthorhombic [18] (Table 2 and Fig. 3). The main difference between the two

Table 2
Single crystal literature data

Phase	Space group	a/Å	b/Å	c/Å	Reference
$Ca_2Fe_2O_5$	Pcmn	5.60	14.77	5.43	[17]
Ca_2AlFeO_5	Ibm2	5.58	14.60	5.37	[18]

structures is that in Ca_2AlFeO_5 all chains of corner-sharing tetrahedra point in the same direction, whereas in $Ca_2Fe_2O_5$ the chain direction alternates between layers perpendicular to the b axis (cf. Figs. 3A and 3B). A phase transformation takes place at $x = 0.3$, where the structure changes from primitive to body-centered symmetry [15,16].

Selected area electron diffraction patterns were used to distinguish the space groups Pcmn and Ibm2 possible for the clinker ferrite with substituting ions (Fig. 4). From the [100] and [010] zone axis spot patterns in Figs. 4A and 4B it can be concluded that the average structure of clinker ferrite has the same symmetry as synthetic Ca_2AlFeO_5, whereas the [001] zone axis pattern in Fig. 4C is of little diagnostic value, as in this case the expected patterns are identical.

2.4. Diffuse scattering

Careful inspection of the diffractograms in Figs. 4A and 4B reveals the presence of diffuse scattering perpendicular to c*. We now have to determine the exact distribution of the diffuse scattering in reciprocal space, and the commonly observed [1 0 −1] zone axis patterns (cf. Figs. 2B and 5A) present an important clue in this respect. Well-aligned diffraction spot patterns are expected to exhibit a center of symmetry at the origin (central spot), but the diffuse features of the electron diffraction pattern in Fig. 5A clearly break the symmetry. The diffuse intensity parallel to b* in the diffraction pattern becomes increasingly displaced relative to the corresponding row of Bragg spots, when rows of higher order are compared with the central row b*, where the diffuse intensity and row of spots coincide perfectly. Compare for example the position of the diffuse intensity close to the reflections [−4 0 4], [0 0 0] (central spot) and [4 0 −4], in Fig. 5A. This behaviour suggests that the diffuse intensity is present in the form of two-dimensional sheets and not in the form of one-dimensional rods.

The displacement of the diffuse scattering to one side in the higher order rows is an effect of the diffuse sheets in diffraction space being inclined by an angle of ∼.45° relative to the primary beam (Fig. 5B). Due to the limited thickness of the crystal, in the beam direction, the Bragg reflections become elongated along the direction of the beam. Diffraction occurs when the sheets and spots in diffraction space cut the Ewald sphere, here represented by a circle segment. As can be seen in Fig. 5B, the intersection with the Ewald sphere of a spot and its corresponding sheet will not coincide, at increasing distances from the central beam. In the figure, the intersection of the sheet is displaced to the right of the intersection of the corresponding spot.

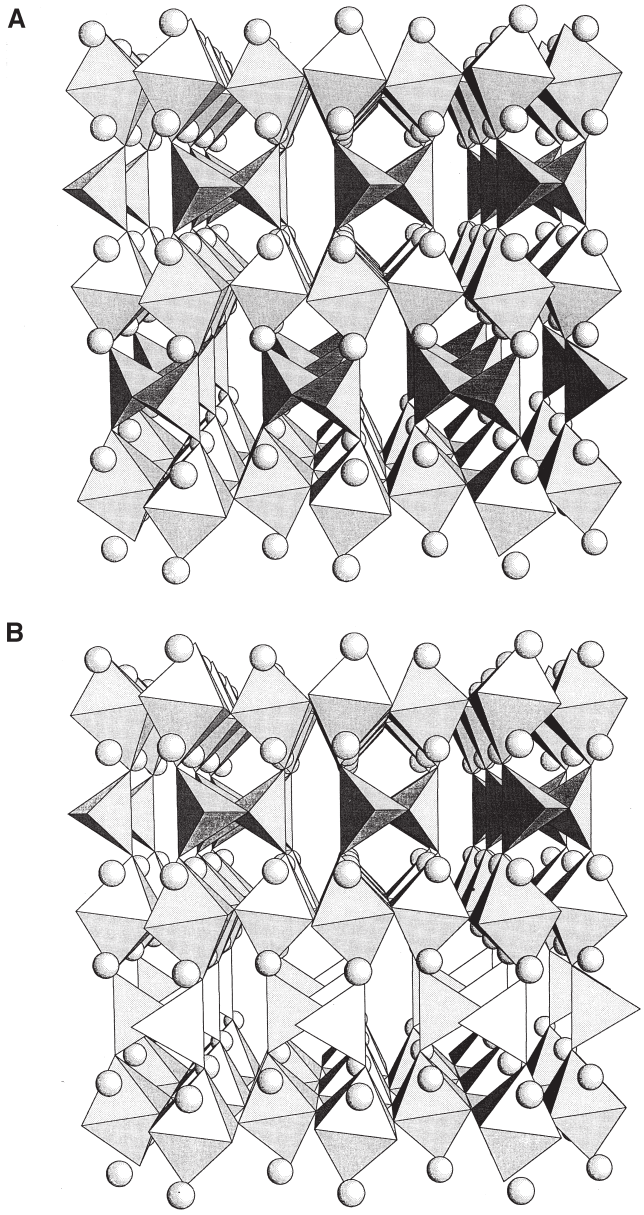

Fig. 3. The crystal structures of (*A*) Ca_2AlFeO_5 and (*B*) $Ca_2Fe_2O_5$ seen along c (a is horizontal and b is vertical). The octahedra are preferentially centred by Fe atoms, the tetrahedra by Al, whereas spheres represent Ca atoms. Oxygens are situated at corners shared by two polyhedra.

To confirm the two-dimensional nature of the diffuse scattering, several series of selected area electron diffraction patterns were recorded while the crystals were being tilted around the b* axis. The row of closely spaced spots along this direction is readily recognised in the microscope. The series of diffraction patterns in Figs. 4A, 6A, and 4C represents a full 90° of tilting, with b* perpendicular to the electron beam and starting with a* parallel to the beam and finishing with c* parallel to the beam. These patterns taken together establish the presence of a more or less continuous sheet of diffuse intensity passing through each consecutive

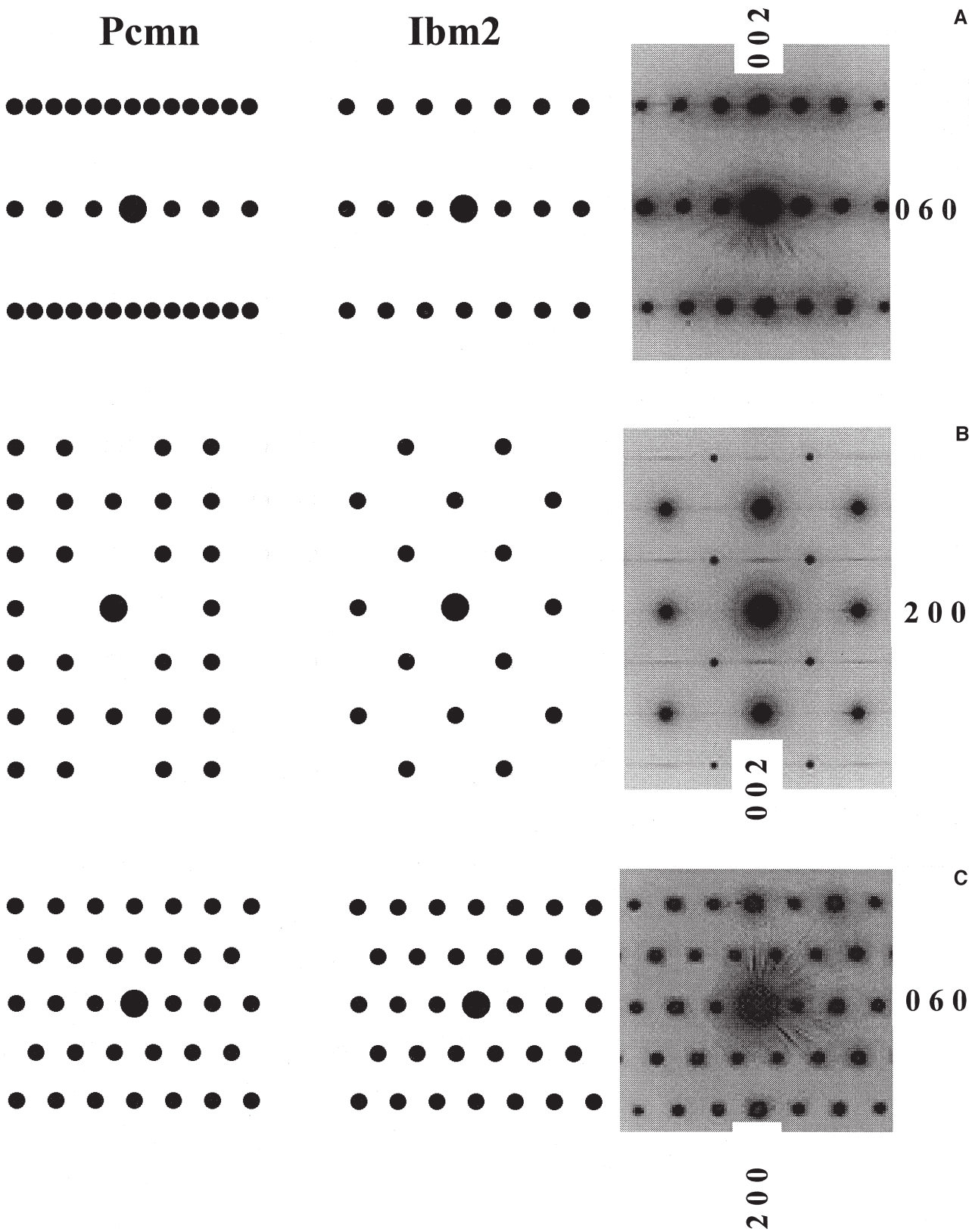

Fig. 4. (Left) Schematic drawings of the expected electron diffraction patterns for symmetry Pcmn and Ibm2; present reflections are represented by filled circles. (Right) The patterns observed using extracted clinker ferrite. Zone axes: (*A*) [1 0 0], (*B*) [0 1 0], (*C*) [0 0 1].

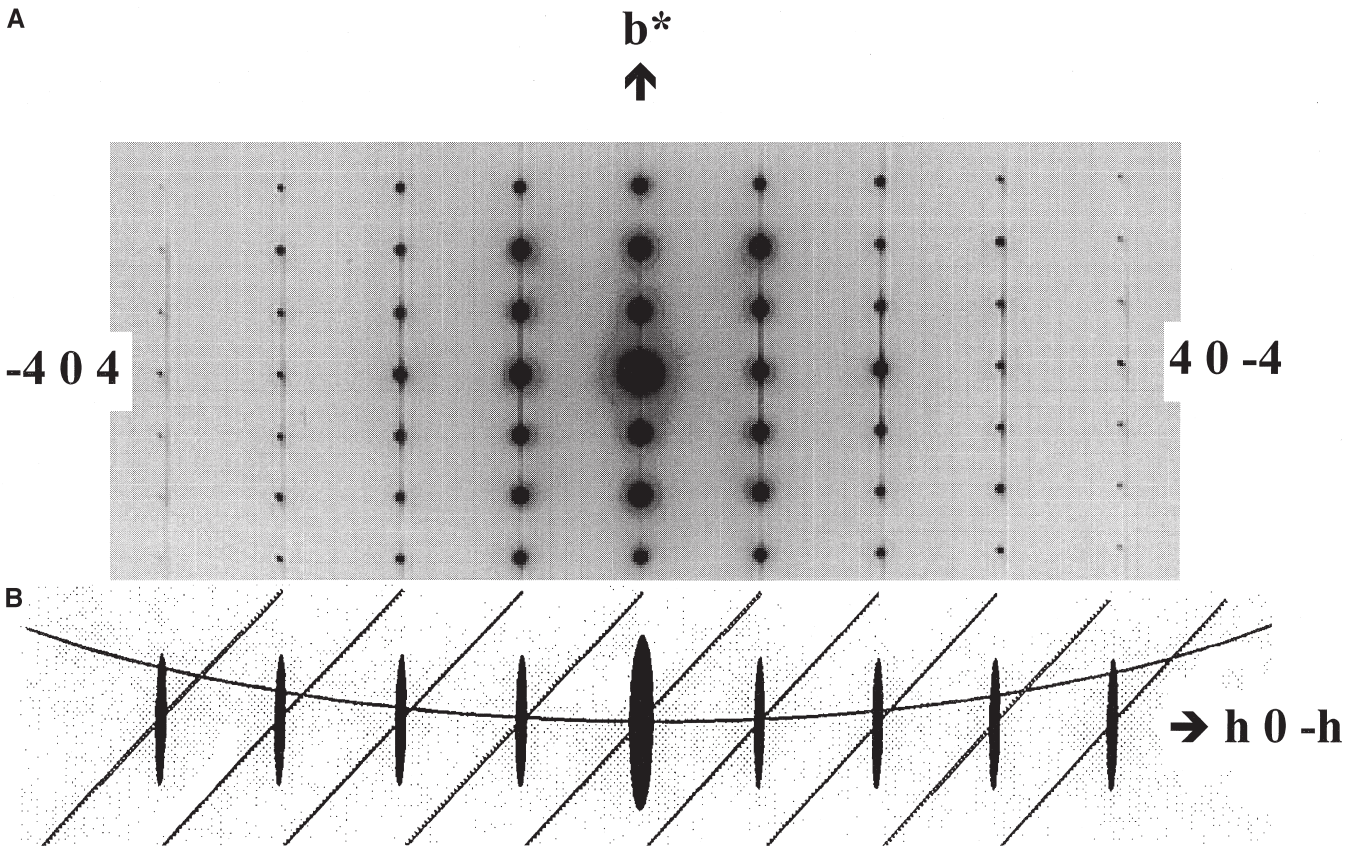

Fig. 5. (*A*) Selected area electron diffraction pattern of a ferrite crystal, with the [1 0 −1] direction oriented along the electron beam, showing diffuse intensity parallel to b*. (*B*) Sideways view (along b*) of the situation in (*A*). Ewald sphere construction showing the origin of gradual displacement of the diffuse intensity relative to the basic reflections; Ewald sphere (curved line), diffuse sheets (inclined lines) and Bragg reflections (filled ellipses). The curvature of the Ewald sphere has been exaggerated for clarity.

layer of Bragg spots perpendicular to c*. This two-dimensional arrangement of diffuse intensity is observed in the individual diffraction patterns as one-dimensional streaks in different positions relative to the basic diffraction spots. In all three of the diffraction patterns (Fig. 6A) rows of Bragg spots parallel to b* are accompanied by diffuse streaks. In the [1 0 −1] zone this is the only type of streak present. The [2 0 −1] zone, on the other hand, shows one additional diffuse streak between the Bragg rows, whereas the [3 0 −1] zone exhibits two extra streaks. How these different types of diffraction pattern are generated is shown in Fig. 6B. Similar sheets of diffuse intensity were reported to occur in electron diffraction experiments performed on the ferrite phase in an oil-well cement clinker [8].

2.5. Extended crystal defects

By analogy with a perfectly ordered, three-dimensional, crystal structure being represented by a set of zero-dimensional spots in diffraction space, a disordered array of one-dimensional crystal defects will give rise to a set of two-dimensional features in diffraction space. Because the observed diffuse sheets are perpendicular to c*, the associated one-dimensional defects must be situated along c in the ordered ferrite matrix, which is represented by the Bragg spots. The occurrence of individual tetrahedral chains with reversed polarity is a type of extended defect, which is well established in perovskite-related cuprates [19] and silica phases [20], and a similar defect model is compatible with the two ferrite crystal structures and the geometry of the observed diffuse scattering in clinker ferrite.

This type of chain disorder has for example been noted in the compounds $(Nd,Ce)Sr_2GaCu_2O_7$ and $YSr_2CoCu_2O_7$ [19]. By analogy with these results, we propose that the diffuse sheets in reciprocal space presented by clinker ferrite are caused by individual chains of tetrahedra pointing in the reverse direction compared to the fully ordered Ca_2AlFeO_5 structure (Fig. 7). The defect chains, with reversed polarity, form a disordered array in the crystal. Some correlation between the chains of switched polarity can be expected to exist though, because the scattered intensity within a sheet exhibits a certain amount of variation (for example, in Fig. 4B).

The role of the substitution $2\,M(3+) \leftrightarrow M(2+) + M(4+)$ in connection with the formation of linear defects remains to be determined, because the positions of the substituting ions are unknown.

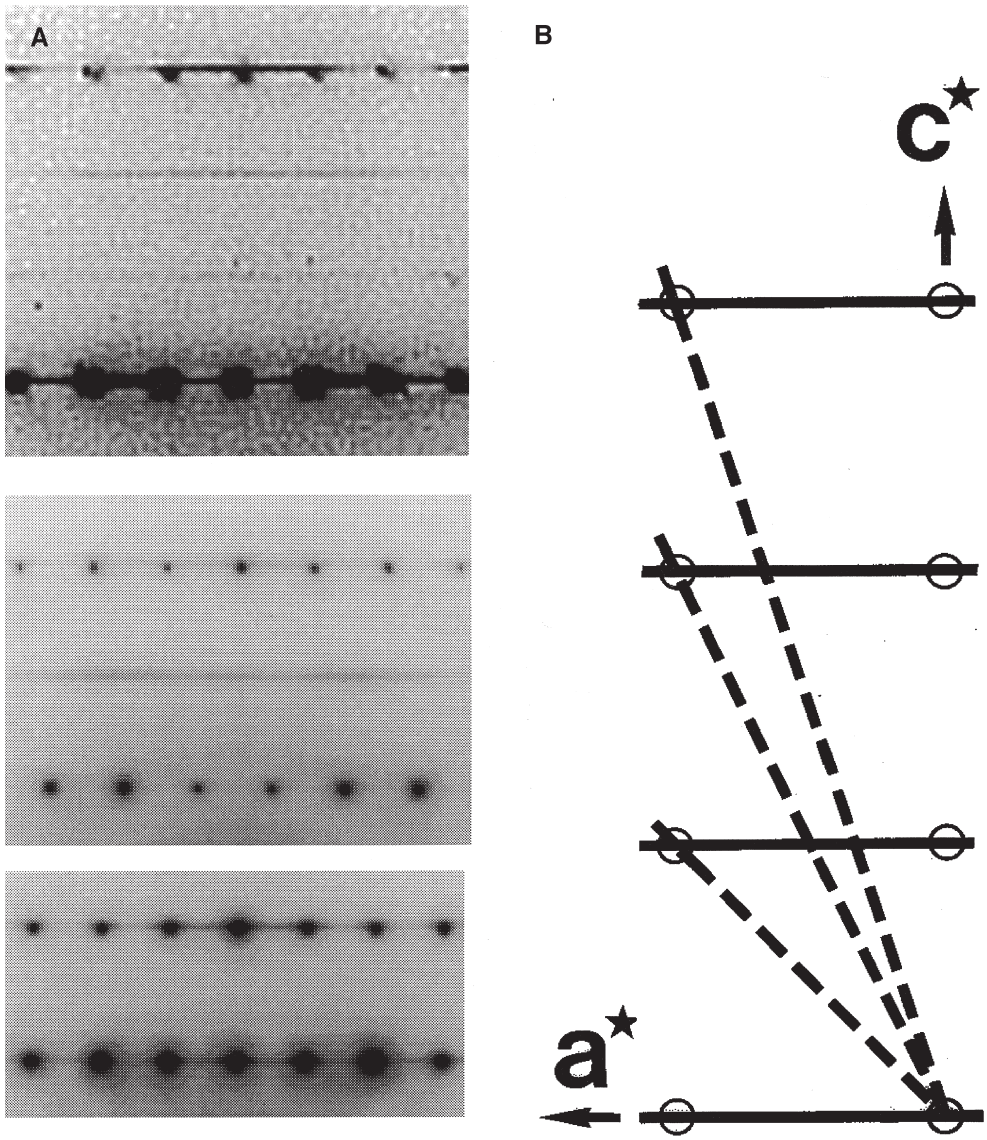

Fig. 6. (*A*) Electron diffraction patterns of ferrite rotated around b* (horizontal in all three diffractograms). Zone axes: top [3 0 −1], middle [2 0 −1], bottom [1 0 −1]. (*B*) Schematic drawing, along b*, of the corresponding Ewald constructions in diffraction space, showing how the Ewald sphere (dashed line) will cut the sheets of diffuse scattering (solid horizontal lines) and Bragg reflections (empty circles) in the three cases displayed in (*A*).

Tetrahedral chains of switched polarity has been proposed to explain the complex diffuse intensity observed in the electron diffraction patterns of high-cristobalite silica [20]. All the SiO_4 tetrahedra in a single chain can undergo a coupled rotation, which does not affect the rest of the framework of corner-connected tetrahedra. Due to symmetry, not less than six intersecting sheets of diffuse intensity were observed.

The crystal structure [21] of the compound $LaCaCuGaO_5$ is closely related to that of Ca_2AlFeO_5, but the direction of the chains of Ga-centered tetrahedra was found to be random. The symmetry used in the refinements corresponds to Ibmm, which is a supergroup of both Pcmn and Ibm2. Streaking along b* was reported, which implies that the crystal defects in this material are two-dimensional slabs.

One-dimensional rods of diffuse scattering parallel to b* were observed by electron diffraction in synthetic samples representing intermediate compositions between Ca_2AlFeO_5 and $Ca_5Al_2Fe_2TiO_{13}$ [22]. The latter phase has a repeat of 18.6 Å along b, and its crystal structure corresponds to the insertion of an extra layer of octahedra and large cations perpendicular to b. This adds one $CaTiO_3$ to each unit cell containing $Ca_4Al_2Fe_2O_{10}$. The intermediate compositions then represent a disordered, mixed-layer stacking in response to the coupled substitution: Fe(3) + Al(3+) + vacancy $\leftrightarrow$ 2 Ti(4+) + O(2−) in the body-centered Ca_2AlFeO_5 phase.

It can be concluded that the extended defects in $LaCaCuGaO_5$ and Ca_2AlFeO_5 doped with TiO_2 are slab-like, whereas the defects in clinker ferrite are rod-like.

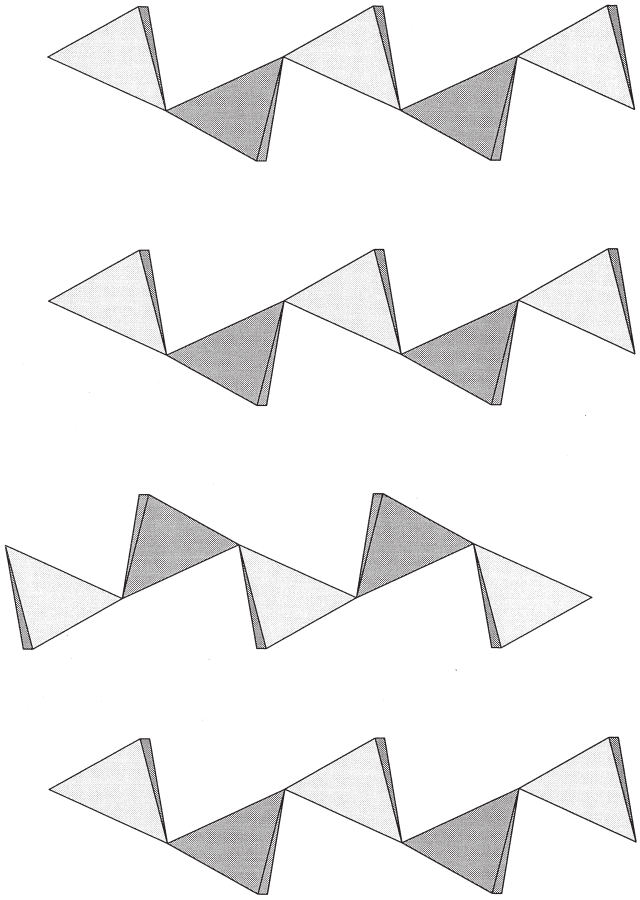

Fig. 7. Proposed model for a slab of tetrahedral chains in ferrite (parallel to the ac plane) exhibiting a single defect chain with reversed orientation along c.

Acknowledgments

The authors wish to thank the Scancem Fund, Cementa AB, and Scancem Research AB for financial support; Scancem Research AB, Slite, for preparing the clinker extracts; and Anna Emanuelson for the determination of lattice constants and for help with image processing.

References

[1] P. Brown, P. Barret, D.D. Double, G. Frohnsdorff, V. Johansen, L.J. Parrot, J.M. Pommersheim, M. Regourd, K. Scrivener, H.F.W. Taylor, J.F. Young, The hydration of tricalcium aluminate and tetracalcium aluminoferrite in the presence of calcium sulfate, Mater Constr 19 (1986) 137–147.

[2] R.S. Gollop, H.F.W. Taylor, Microstructural and microanalytical studies of sulfate attack. I. Ordinary portland cement paste, Cem Concr Res 22 (1992) 1027–1038.

[3] R.S. Gollop, H.F.W. Taylor, Microstructural and microanalytical studies of sulfate attack. II. Sulfate-resisting portland cement: ferrite composition and hydration chemistry, Cem Concr Res 24 (1994) 1347–1358.

[4] A. Emanuelson, E. Henderson, S. Hansen, Hydration of ferrite Ca_2AlFeO_5 in the presence of sulphates and bases, Cem Concr Res 26 (1996) 1689–1694.

[5] A. Emanuelson, S. Hansen, Distribution of iron among ferrite hydrates, Cem Concr Res 27 (1997) 1167–1177.

[6] A. Emanuelson, S. Hansen, E. Henderson, A. Landa-Cánovas, E. Sjöstedt, Ferrite—Microstructure in clinker and hydration of synthetic phases and sulphate resisting cements, in: H. Justnes (Ed.), Proc 10th Int Congr Chem Cem, volume 1, Göteborg, Amaraki AB and Congrex Göteborg AB, 1997, paper 1i060.

[7] E. Bäckström, S. Hansen, X-ray mapping of interstitial phases in sulphate resisting cement clinker, Adv Cem Res 9 (1997) 17–23.

[8] I.G. Richardson, C. Hall, G.W. Groves, TEM study of the composition of the interstitial phase in an oil-well cement clinker, Adv Cem Res 5 (1993) 15–21.

[9] T.B. Bergström, C. Hall, K.L. Scrivener, Interstitial material in oil-well cements: Evidence from x-ray microanalysis, Adv Cem Res 4 (1991/1992) 141–147.

[10] F. Puertas, M.T. Blanco Varela, R. Dominguez, Characterization of Ca_2AlMnO_5. A comparative study between Ca_2AlMnO_5 and Ca_2AlFeO_5, Cem Concr Res 20 (1990) 429–438.

[11] M. Maultzsch, H. Scholze, Formation of the ferritic clinker phase from the melt, Zem-Kalk-Gips 26 (1973) 583–587.

[12] M.C. Ball, R.E. Simmons, I. Sutherland, Surface composition of anhydrous tricalcium aluminate and calcium aluminoferrite, J Mater Sci 22 (1987) 1975–1979.

[13] A. Negro, L. Stafferi, The hydration of calcium ferrites and calcium aluminoferrites, Zem-Kalk-Gips 32 (1979) 83–88.

[14] J. Neubauer, R. Sieber, H.-J. Kuzel, M. Ecker, Investigations on introducing Si and Mg into brownmillerite—A Rietveld refinement, Cem Concr Res 26 (1996) 77–82.

[15] D.K. Smith, Crystallographic changes with the substitution of aluminum for iron in dicalcium ferrite, Acta Crystallogr 15 (1962) 1146–1152.

[16] F. Guirado, S. Gali, S. Chinchón, X-ray profile analysis of $Ca_2Fe_{2-x}Al_xO_5$ solid solutions, World Cement 12 (1996) 73–76.

[17] A.A. Colville, The crystal structure of $Ca_2Fe_2O_5$ and its relation to the nuclear electric field gradient at the iron sites, Acta Crystallogr B 26 (1970) 1469–1473.

[18] A.A. Colville, S. Geller, The crystal structure of brownmillerite, Ca_2FeAlO_5, Acta Crystallogr B 27 (1971) 2311–2315.

[19] O. Milat, T. Krekels, G. van Tendeloo, S. Amelinckx, Ordering principles for tetrahedral chains in Ga- and Co-substituted YBCO intergrowths, J Phys I France 3 (1993) 1219–1234.

[20] G.L. Hua, T.R. Welberry, R.L. Withers, J.G. Thompson, An electron diffraction and lattice-dynamical study of the diffuse scattering in β-cristobalite, SiO_2, J Appl Cryst 21 (1988) 458–465.

[21] A.L. Kharlanov, I. Bryntse, E.V. Antipov, A. Luzikova, The crystal structure of the brownmillerite-related phase $LaCaCuGaO_5$, Acta Chem Scand 47 (1993) 434–438.

[22] M.B. Marinho, F.P Glasser, Polymorphism and phase changes in the ferrite phase of cements induced by titanium substitution, Cem Concr Res 14 (1984) 360–368.